Applied Catalysis B: Environmental 88 (2009) 438–447

Contents lists available at ScienceDirect

Applied Catalysis B: Environmental

journal homepage: www.elsevier.com/locate/apcatb

$La_{(1-x)}Sr_xCo_{1-y}Fe_yO_3$ perovskites prepared by sol–gel method: Characterization and relationships with catalytic properties for total oxidation of toluene

S. Rousseau, S. Loridant *, P. Delichere, A. Boreave, J.P. Deloume, P. Vernoux

Institut de Recherches sur la Catalyse et l'Environnement de Lyon (IRCELYON), CNRS-Université Claude Bernard Lyon 1, 2 av. A. Einstein, F-69626 Villeurbanne Cedex, France

ARTICLE INFO

Article history:
Received 11 July 2008
Received in revised form 22 October 2008
Accepted 25 October 2008
Available online 8 November 2008

Keywords:
$La_{(1-x)}Sr_xCo_{(1-y)}Fe_yO_3$
Perovskite
Sol–gel method
Toluene total oxidation
VOC abatement
Raman mappings
XPS
Mössbauer spectroscopy
O^- species
Co_3O_4

ABSTRACT

$La_{(1-x)}Sr_xCo_{(1-y)}Fe_yO_3$ samples have been prepared by sol–gel method using EDTA and citric acid as complexing agents. For the first time, Raman mappings were achieved on this type of samples especially to look for traces of Co_3O_4 that can be present as additional phase and not detect by XRD. The prepared samples were pure perovskites with good structural homogeneity. All these perovskites were very active for total oxidation of toluene above 200 °C. The ageing procedure used indicated good thermal stability of the samples. A strong improvement of catalytic properties was obtained substituting 30% of La^{3+} by Sr^{2+} cations and a slight additional improvement was observed substituting 20% of cobalt by iron. Hence, the optimized composition was $La_{0.7}Sr_{0.3}Co_{0.8}Fe_{0.2}O_3$. The samples were also characterized by BET measurements, SEM and XRD techniques. Iron oxidation states were determined by Mössbauer spectroscopy. Cobalt oxidation states and the amount of O^- electrophilic species were analyzed from XPS achieved after treatment without re-exposition to ambient air. Textural characterization revealed a strong increase in the specific surface area and a complete change of the shape of primary particles substituting La^{3+} by Sr^{2+}. The strong lowering of the temperature at conversion 20% for the $La_{0.7}Sr_{0.3}Co_{(1-y)}Fe_yO_3$ samples can be explained by these changes. X photoelectron spectra obtained with our procedure evidenced very high amount of O^- electrophilic species for the $La_{0.7}Sr_{0.3}Co_{(1-y)}Fe_yO_3$ samples. These species able to activate hydrocarbons could be the active sites. The partial substitution of cobalt by iron has only a limited effect on the textural properties and the amount of O^- species. However, Raman spectroscopy revealed a strong dynamic structural distortion by Jahn–Teller effect and Mössbauer spectroscopy evidenced the presence of Fe^{4+} cations in the iron containing samples. These structural modifications could improve the reactivity of the active sites explaining the better specific activity rate of the $La_{0.7}Sr_{0.3}Co_{0.8}Fe_{0.2}O_3$ sample. Finally, an additional improvement of catalytic properties was obtained by the addition of 5% of cobalt cations in the solution of preparation. As evidenced by Raman mappings and TEM images, this method of preparation allowed to well-dispersed small Co_3O_4 particles that are very efficient for total oxidation of toluene with good thermal stability contrary to bulk Co_3O_4.

1. Introduction

Noble metals, such as Pt and Pd, are the most effective catalysts for hydrocarbon and volatile organic compounds (VOCs) deep oxidation. In spite of their high efficiency, noble metal catalysts cannot be considered for a medium range future because of their excessive cost which makes necessary stages of recovery and recycling [1]. Most promising alternative catalysts seem to be perovskite oxides with the general formula ABO_3. For instance, lanthanum manganites with perovskite structure were known as active oxide catalysts for the deep oxidation of methane. The catalytic performances of such oxides are generally related to their specific surface area which strongly depends on the synthesis conditions. However, the surface area is not the only factor which governs the catalytic activity of these catalysts. The stability of the perovskite structure allows partial substitution on both the A and B cation sites. These substitutions generally enhance the activity of the catalyst [1]. In some case, substituted lanthanum manganites can reach the same activity as noble metals [2]. Arai et al. reported that $La_{0.6}Sr_{0.4}MnO_3$ can exhibit higher activity for methane combustion than $LaMnO_3$ [2] and also did Batis et al. for $La_{0.4}Ca_{0.6}MnO_3$ [3]. Two mechanisms involving two kinds of oxygen species are proposed in the literature for hydrocarbon oxidation on perovskite materials: intrafacial and suprafacial [4],

* Corresponding author. Tel.: +33 4 72445334; fax: +33 4 72445399.
E-mail address: stephane.loridant@ircelyon.univ-lyon1.fr (S. Loridant).

0926-3373/$ – see front matter © 2008 Elsevier B.V. All rights reserved.
doi:10.1016/j.apcatb.2008.10.022

depending on the operating temperatures. The suprafacial mechanism prevails at low temperatures (300 °C) and involves the reaction of surface oxygen adsorbed on the catalyst. The presence of weakly bonded O^- species associated with anion vacancies induced by the lattice non-stoichiometry of the perovskite was reported and evidenced by XPS on $LaCoO_3$ perovskites [5]. On the other hand, the intrafacial mechanism occurs at high temperatures (600 °C) when the concentration of adsorbed species becomes low. Bulk oxygen species coming from the perovskite lattice are assumed to be more active and react with hydrocarbons.

The abatement of volatile organic compounds by catalytic deep oxidation takes part in the major preoccupations concerning global air purification. Efforts to improve air quality were successfully performed for many years in industrial processes. Among the large varieties of VOC, toluene can be considered as representative of aromatic hydrocarbons. Only few studies are reported in the literature despite its ability to be oxidized on perovskite without formation of secondary products compared to other VOCs [6]. The toluene total oxidation over perovskites such as $LaCoO_3$ and $LaMnO_3$ has been investigated [7]. It was found that cobaltite perovskites are more efficient for this reaction than manganites. Moreover, it was observed that partial substitution of lanthanum with strontium, $La_{1-x}Sr_xCoO_3$, can significantly improve the catalytic activity [7–9]. Additionally, several studies on total oxidation of alkanes indicate that the partial substitution of cobalt cations with another metal such as iron leads to significant activity improvement attributed to more reactive chemisorbed oxygen species [10,11].

Nevertheless, the intrinsic activity of the perovskite is difficult to clearly evidence mainly because of relatively low specific surface areas and/or presence of undesired impurities like carbonates or oxides (e.g. Co_3O_4) [8,12,14]. These two parameters strongly depend on the preparation method as well as the calcination procedure for achieving the crystallized perovskite phase. Citrate method is probably the most widespread and the most effective route to create higher surface areas. Additionally, the decomposition of the amorphous citrate precursors leads to mixed oxides or solid solutions of high homogeneity [15] contrary to methods using hydroxide precursors for instance [16].

The aim of this work was to prepare well-defined lanthanum cobalt perovskites using the citrate method, evaluate their catalytic properties for toluene total oxidation and establish relationships with physico-chemical properties. Various compositions, with partial substitutions of both La and Co by Sr and Fe, respectively, were prepared in order to determine the most efficient formulation for toluene deep oxidation. Additionally, a severe ageing procedure was used to measure the thermal stability of the samples. The samples were characterized by BET, SEM and XRD techniques. Additionally, the purity of the prepared samples has been carefully controlled by micro-Raman spectroscopy achieving several mappings. This technique used for the first time on this system is powerful to detect traces of Co_3O_4. Iron oxidation states were determined by Mössbauer. X photoelectron spectra achieved after treatment without re-exposition to ambient air allowed quantification of the amount of O^- electrophilic species. Comparison with data obtained without treatment underlines the interest of such treatment. Finally, the amount of cobalt precursor was varied around the optimized composition to prepare a catalyst presenting an excess or a deficiency of Co. An excess of 5% of Co improved catalytic properties. This was explained from TEM images and Raman mappings by the additional presence of well-dispersed small Co_3O_4 particles that have good thermal stability.

2. Experimental methods

2.1. Catalysts preparation

A series of $La_{1-x}Sr_xCo_{1-y}Fe_yO_3$ perovskite-type compounds was synthesized by a combined citrate–EDTA complexing method [17]. After determining the metal content of the hygroscopic nitrates by a titration method, the stoichiometric amounts of $Co(NO_3)_2{\cdot}6H_2O$, $Fe(NO_3)_3{\cdot}9H_2O$, $Sr(NO_3)_2$ and $La(NO_3)_3{\cdot}6H_2O$ were dissolved in EDTA–citric acid–$NH_3{\cdot}H_2O$ solution under heating and stirring. The mole ratio of EDTA:citric acid:total metal ions was 1:1.5:1. x was varied from 0 to 0.3 and y from 0 to 0.5 to optimize the perovskite composition. Samples were also prepared with deficiency or excess of 5% Co and will be labelled $La_{1-x}Sr_xCo_{1-y}Fe_yO_3$ (−5% Co) and $La_{1-x}Sr_xCo_{1-y}Fe_yO_3$ (+5% Co) in the following. After stirring to get good homogeneity, concentrated NH_4OH was introduced to obtain a pH value around 9. With the evaporation of water, a dark purple concentrated solution was obtained. It was then dried in an oven at 120–150 °C overnight. The solid black foam obtained was finely ground and calcined under flowing air at first at 450 °C for 4 h to decompose nitrates and second at 800 °C for 2 h. The final temperature was chosen for insuring thermal stability during catalytic activity measurements. Catalytic properties of commercial Co_3O_4 powder (Alfa-Aesar) were also evaluated.

2.2. Catalysts characterization

XRD patterns of catalyst samples were recorded with a Siemens D5005 powder X-ray diffractometer using the Ni-filtered Cu Kα (λ = 1.5418 Å) as radiation source. The $K_{\alpha 2}$ contribution to the diagrams was stricken with the EVA software (Bruker-AXS). Crystalline phases were identified by comparison with reference patterns from the JCPDS database. The average crystallite size was calculated by means of the Scherrer formula: $D = K\lambda/(\beta \cos\theta)$ after Warren's correction for instrumental broadening. K was taken equal to 1 and λ corresponded to the wavelength of the $K_{\alpha 1}$ line (1.5406 Å). β was the effective linewidth of the X-ray reflexion, calculated by means of the formula: $\beta^2 = (\beta_{mes})^2 - (\beta_{instr})^2$, where β_{mes} was the measured FWHM of the (0 2 4) peak at $2\theta = 47°$ and the instrumental width β_{instr} was $(0.07\pi/180)$ rd.

BET specific surface areas (SSAs) were determined by nitrogen adsorption at the liquid nitrogen temperature (−196 °C) on a Micromeritics ASAP 2020 instrument. Before each adsorption, the catalyst powder was degassed for 3 h at 300 °C under vacuum of typically 10^{-3} Pa in order to remove adsorbed species.

Raman spectra were recorded at room temperature using a LabRam HR (Jobin Yvon–Horiba) spectrometer equipped with a CCD detector cooled at −75 °C. Measurements were carried out under microscope with a 100× objective that focused the laser beam on the sample surface and collected the scattered light. The exciting line at 514.53 nm of a 2018RM Ar^+/Kr^+ laser (Spectra Physics) was used with a limited power of 100 μW. It was previously checked that the laser heating of the samples was negligible with such a power. A low dispersion grating of 300 grooves/mm was chosen to get a maximum signal. Using such grating, the positions of bands were accurate to within 4 cm^{-1}. Three Raman mappings of 30 analysis points were systematically achieved with a motorized plate to control the homogeneity and purity of both the prepared and the tested compounds. This technique is especially very powerful to detect the presence of small amounts of Co_3O_4 that cannot be detected by XRD thanks to the Raman response of this phase and the spatial resolution under microscope (typically 1 μm with a 100× objective). The spectra were recorded and treated using the Labspec software (Jobin Yvon).

Scanning electron microscopy (SEM) micrographs were obtained with a Hitachi S800 FEG apparatus applying an acceleration voltage of 15 kV. The samples were firstly deposited on a carbon self-adhesive tape that was then stuck on an aluminium holder and coated by a gold film using cathodic pulverisation.

High-resolution electron microscopy was achieved with a JEOL 2010 LaB6 microscope. The acceleration voltage was 200 kV with LaB_6 emission current and the point resolution was 0.19 nm. The samples were previously dispersed in ethanol using ultrasonic bath and then deposited on holey carbon coated 200 mesh, Cu, PK/100 grid.

Mössbauer spectroscopy was conducted at room temperature in ambient air using ^{57}Co/Rh as the γ-ray source and a conventional constant acceleration Mössbauer spectrometer. The isomer shifts are given with respect to α-Fe. The areas of the observed signals have been used to evaluate the relative populations of the different iron species, assuming an equal free recoil fraction for all species.

XPS was performed in a Kratos Axis Ultra DLD equipped with a magnetic immersion lens, a hemispherical analyzer and a delay line detector. The base pressure in the analysis chamber was better than 5×10^{-8} Pa. XPS spectra of O 1s, C 1s, Sr 3d, Co 2p and La 3d levels were measured at 90° (normal angle with respect to the plane of the surface) using a monochromated Al Kα X-ray source, with a pass energy of 20 eV and a spot size aperture of 300 μm × 700 μm. A charge neutraliser was used to control charges effects on samples. Before surface analysis, the catalysts were heated at 600 °C under air (1 bar) for 2 h in a high temperature gas reaction cell. The heat source was a radiative boron nitride heating plate above the quartz reaction vessel. After the treatment, samples were transferred under UHV directly into the XPS analysis chamber. A $La_{0.7}Sr_{0.3}Co_{0.8}Fe_{0.2}O_3$ sample was also characterized without treatment for comparison.

2.3. Catalytic properties

Catalytic measurements were performed at atmospheric pressure in a conventional U-shaped tubular reactor placed in a tubular furnace. The catalyst sample (about 400 mg) was deposited on a quartz wool plug. The reaction temperature was measured with a K-type thermocouple located inside the catalytic bed. The reactive mixture was composed of toluene vapour (500 ppmv), O_2 (20%, Air Liquide, 99.995% purity) and completed with He (79.5%, Air Liquide, 99.995% purity) used as carrier gas. In order to adjust the VOC concentration, two He streams were employed: the first one was introduced into a regulated saturator to maintain a constant flow rate of toluene vapour and the other one balanced the overall concentration.

The overall gas-flow rate was kept constant at 100 mL min^{-1} and the mass of catalyst was 400 mg. The corresponding space velocity was 5700 h^{-1}. The gas composition was controlled by Brooks mass flow meters. The samples were previously pretreated at 600 °C for 2 h under O_2 flow to remove residual carbonates.

The reactant and product gases were analyzed by an on-line gas chromatograph (Perkin Elmer Clarus 500) equipped with a thermal conductivity detector (TCD) and several columms (Shin Carbon ST, Q PLOT, 2 OV101 and molecular sieve) to separate toluene, O_2, CO_2 and CO. The detection limit was 2 ppmv for carbon dioxide and no other product was detected. After checking that toluene conversion and CO_2 yield were very close, the CO_2 peak was used to calculate the conversions. A PC with dedicated program controlled the valve injection system, data acquisition and the integration of chromatographic peaks. Blank experiments have shown that the quartz reactor was catalytically inert at least up to 600 °C.

Catalytic performances of the prepared perovskites for the deep oxidation of toluene were evaluated on fresh catalysts, i.e. as prepared materials, and for aged ones, i.e. after 6 h on stream at 600 °C. This ageing procedure was performed at relatively high temperature for a VOC abatement application and can be considered as a fast experiment for simulating long-term stability of the catalysts. Two parameters will be used to describe and compare the catalytic activities of the various samples:

- The T_{20} value is the temperature corresponding to 20% conversion of toluene for fresh and aged catalysts (Table 3).
- The r specific catalytic rate, expressed in moles of consumed toluene per square meter and second. The r values are compared at 220 °C (Table 3).

3. Results and discussion

3.1. Physico-chemical characterization

The XRD patterns of the various samples calcined at 800 °C are plotted in Fig. 1. They all reveal the presence of a single phase with rhombohedral distorted perovskite structure and a space group $R\bar{3}c$. Traces of a $Sr(CO_3)$ phase can be identified at 25.3° (2Θ) for the samples containing 30% of strontium and reflect the high ability of strontium to carbonation in ambient atmosphere. No reflection of iron oxides was observed by XRD suggesting incorporation of iron into the perovskite structure. Although 5% of Co was added in the $La_{0.7}Sr_{0.3}Co_{0.8}Fe_{0.2}O_3$ (+5%) sample, no evidence of the presence of Co_3O_4 phase was obtained by XRD. Nevertheless, the presence of small amount of Co_3O_4 cannot be ruled out from the XRD diagram since the response of this crystalline phase is low.

The unit cell parameters of the $R\bar{3}c$ structure were refined with the Fullprof software [18]. The results are summarized in Table 1. The values obtained both for $LaCoO_3$ or $La_{0.7}Sr_{0.3}CoO_3$ samples are in good agreement with the literature [19–21]. The substitution of La^{3+} by Sr^{2+} cations led to an increase in the unit cell volume and the c parameter due to a slightly higher ionic radius ($r_{La^{3+}} = 1.36$ Å, $r_{Sr^{2+}} = 1.44$ Å, in dodecahedral coordination) [22]. Nevertheless, the a parameter was slightly lower for the $La_{0.7}Sr_{0.3}CoO_3$ sample. It could arise from the formation of small amount of Co^{4+} cations that have a smaller ionic radius than Co^{3+} [21]. Interestingly, substitution of cobalt by iron gives rise to a significant increase in the a, c and unit cell volume parameters as reported by Trofimenko and Ullmann for $Sr_{(1-x)}Ce_xFe_{(1-y)}Co_yO_{(3-\delta)}$ perovskites [23]. However, only small increases are expected considering the ionic radii of Co^{3+} and Fe^{3+} in the low spin state (0.545 and 0.55 Å, respectively) [22]. Hence, such enhancements could reveal high spin states of Co^{3+} ($r_{Co^{3+}} = 0.61$ Å), Fe^{3+} ($r_{Fe^{3+}} = 0.645$ Å) [22] or the presence of Fe^{4+} ($r_{Fe^{4+}} = 0.585$ Å) [22]. Finally, neither the addition of an excess of Co nor the Co deficiency seems to affect the unit cell parameters of the perovskite.

The D average size of the particles was calculated from the Scherrer equation using the (0 2 4) peak. The results are reported in Table 1. Partial substitution of cobalt by iron cations had only a limited effect on the D value whereas partial substitution of lanthanum by strontium cations led to a significant decrease. The $La_{0.7}Sr_{0.3}Co_{0.8}Fe_{0.2}O_3$ and $La_{0.7}Sr_{0.3}Co_{0.8}Fe_{0.2}O_3$ (−5% Co) samples exhibit an average particle size of ∼20 nm whereas a much larger crystallite size (∼30 nm) was obtained with the $La_{0.7}Sr_{0.3}Co_{0.8}Fe_{0.2}O_3$ (+5% Co) sample.

The specific surface areas of the samples are gathered in Table 1. Partial substitution of lanthanum by strontium cations led to a strong increase in the surface area whereas partial substitution of cobalt by iron cations up to 20% slightly increased the surface.

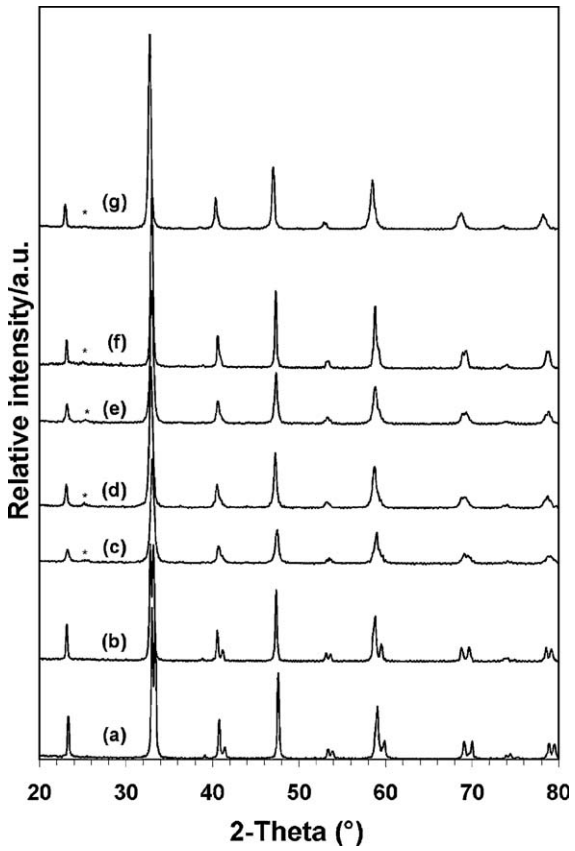

Fig. 1. X-ray diffraction patterns of the (a) $LaCoO_3$, (b) $LaCo_{0.8}Fe_{0.2}O_3$, (c) $La_{0.7}Sr_{0.3}CoO_3$, (d) $La_{0.7}Sr_{0.3}Co_{0.8}Fe_{0.2}O_3$ (−5% Co), (e) $La_{0.7}Sr_{0.3}Co_{0.8}Fe_{0.2}O_3$, (f) $La_{0.7}Sr_{0.3}Co_{0.8}Fe_{0.2}O_3$ (+5% Co) and (g) $La_{0.7}Sr_{0.3}Co_{0.5}Fe_{0.5}O_3$ samples.

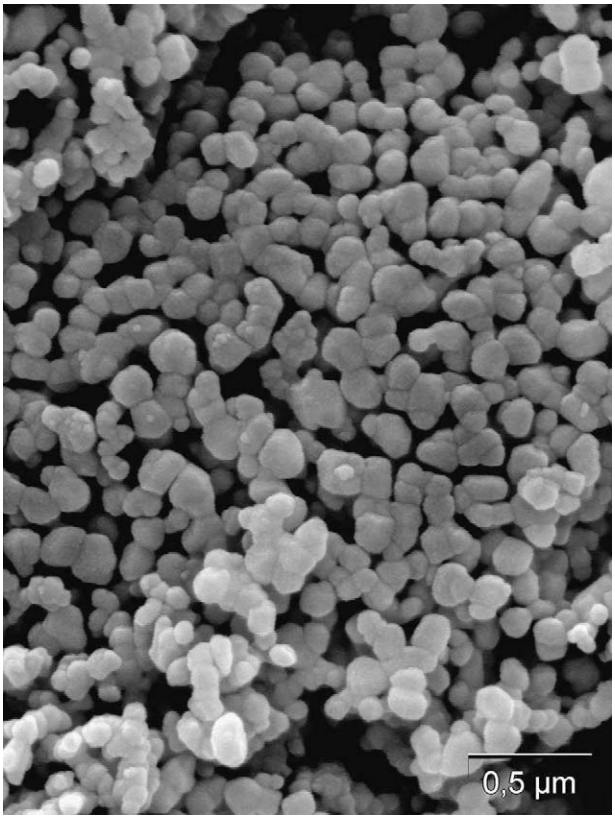

Fig. 2. SEM micrograph of the $LaCoO_3$ sample.

Hence, the highest SSA was obtained for the $La_{0.7}Sr_{0.3}Co_{0.8}Fe_{0.2}O_3$ sample. Addition of 5% Co during preparation of $La_{0.7}Sr_{0.3}Co_{0.8}$-$Fe_{0.2}O_3$ led to a drastic decrease in the SSA. The variations of SSA are overall in agreement with those of the crystallite size *D* deduced from XRD diagrams. However, SSA did not vary exactly as $1/D$ suggesting differences of particles morphology from one sample to the other.

Scanning electron microscopy was used to determine the microstructural changes with the perovskite formulation. The $LaCoO_3$ sample contained primary particles of around 100 nm with a rather spherical shape (Fig. 2). The same shape was observed for the $LaCo_{0.8}Fe_{0.2}O_3$ sample but primary particles were much thinner (Fig. 3). Substitution of La^{3+} by Sr^{2+} cations led to very small primary particles with fluffy morphology in agreement with the strong increase in the surface area (Figs. 4 and 5). No significant change in the shape or in the size of the primary particles was observed varying the cobalt stoichiometry.

Raman spectroscopy is a powerful technique to probe dynamic local distortions that cannot be detected by diffraction [24]. Additionally, the structural and chemical homogeneity can be checked analyzing various areas of the samples under microscope with a probe of around 1 μm. In particular, this technique is much more efficient than XRD to detect traces of Co_3O_4 because of its high scattering cross-section. Such a control is crucial since Co_3O_4 is active catalyst for total oxidation of hydrocarbons [25,26] and hence its presence even in small amount can influence the catalytic activity. In this way, a first series of samples was prepared without titration of the nitrates precursors. The presence of Co_3O_4 crystallites was never detected by XRD. As illustrated in Fig. 6a by the image plotting the spatial distribution of the intensity of the main band of Co_3O_4 at 690 cm^{-1}, micro-Raman spectroscopy revealed the presence of traces of this crystalline phase in the $La_{0.7}Sr_{0.3}Co_{0.8}Fe_{0.2}O_3$ sample of this series.

As we preferred to determine the catalytic activities of pure perovskites, a second series was prepared controlling carefully cobalt stoichiometry by titration of nitrate precursors. No Co_3O_4 was detected in all the Raman mappings achieved for the series. Indeed, the intensity of the band at 690 cm^{-1} was close to zero for all the analyzed points as it is illustrated for the $La_{0.7}Sr_{0.3}Co_{0.8}$-$Fe_{0.2}O_3$ sample in Fig. 6b. The only exception was the $La_{0.7}Sr_{0.3}$-

Table 1
Physico-chemical properties of the various samples.

Sample	*a* (Å)	*c* (Å)	Unit cell volume (nm^3)	*D* (nm)	SSA ($m^2\ g^{-1}$)
$LaCoO_3$	5.4404	13.112	0.3361	33.3	7.4
$LaCo_{0.8}Fe_{0.2}O_3$	5.4516	13.146	0.3384	31.6	9.6
$La_{0.7}Sr_{0.3}CoO_3$	5.4357	13.186	0.3374	16.6	17.1
$La_{0.7}Sr_{0.3}Co_{0.8}Fe_{0.2}O_3$ (−5% Co)	5.4481	13.217	0.3397	21.6	18.3
$La_{0.7}Sr_{0.3}Co_{0.8}Fe_{0.2}O_3$	5.4471	13.224	0.3398	20.7	22.2
$La_{0.7}Sr_{0.3}Co_{0.8}Fe_{0.2}O_3$ (+5% Co)	5.4406	13.227	0.3391	30.6	10.0
$La_{0.7}Sr_{0.3}Co_{0.5}Fe_{0.5}O_3$	5.4590	13.368	0.3450	22.7	14.8

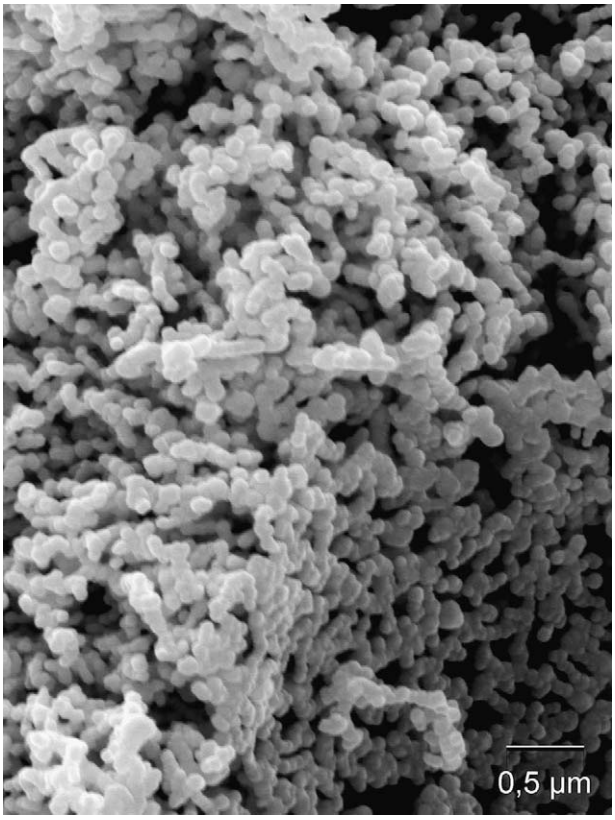

Fig. 3. SEM micrograph of the $LaCo_{0.8}Fe_{0.2}O_3$ sample.

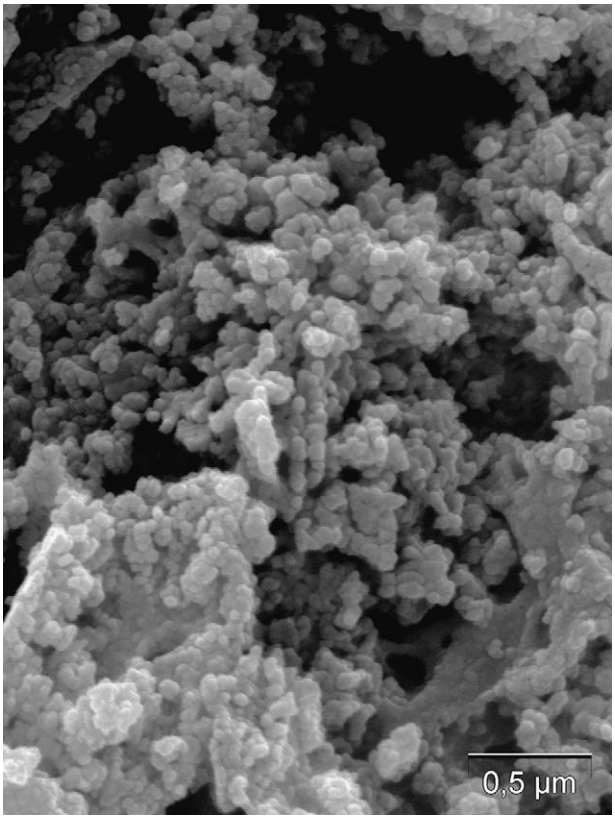

Fig. 5. SEM micrograph of the $La_{0.7}Sr_{0.3}Co_{0.8}Fe_{0.2}O_3$ sample.

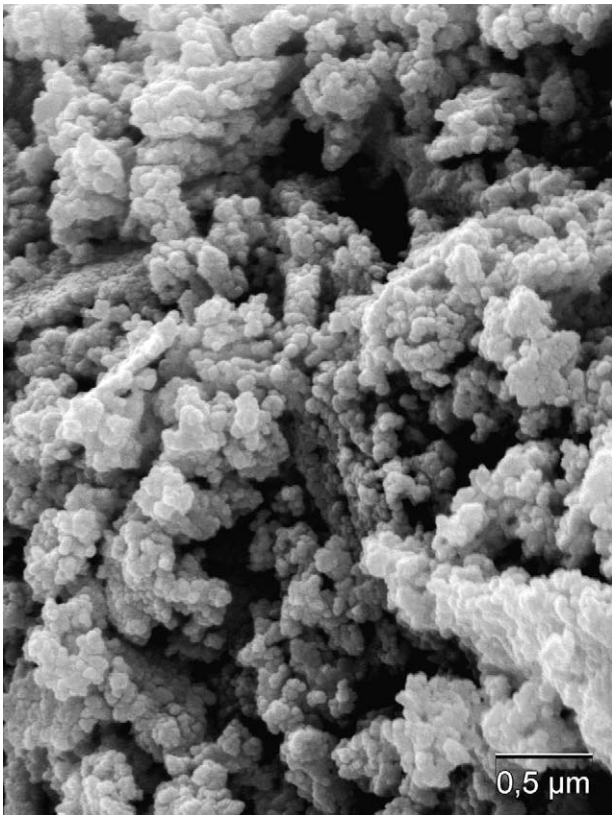

Fig. 4. SEM micrograph of the $La_{0.7}Sr_{0.3}CoO_3$ sample.

$Co_{0.8}Fe_{0.2}O_3$ (+5% Co) sample which contained voluntarily an excess of cobalt cations. For this sample, the bands at 480, 520, 620 and 690 cm^{-1} typical of the spinel structure of Co_3O_4 [28] were observed for almost each analyzed point indicating a rather good dispersion of the additional phase. Fig. 7f which reports the mean spectrum of this sample shows that the relative intensity of Co_3O_4 was high. Fig. 8 shows a TEM image of the $La_{0.7}Sr_{0.3}Co_{0.8}Fe_{0.2}O_3$ (+5% Co) sample evidencing a perovskite crystallite inlayed at a corner by a spherical particle of ca 30 nm. EDX measurements achieved with a probe of 10 nm revealed that this spherical particle was cobalt oxide. Only isolated cobalt oxide particles were evidenced during the TEM examination confirming good dispersion of this additional phase.

Factor group analysis of perovskites with the $R\bar{3}c$ (D^6_{3d}, $Z = 2$) space group reveals that 18 optical phonons of irreducible representations $A_{1g} + 3A_{2g} + 2A_{1u} + 3A_{2u} + 4E_g + 5E_u$ are expected. Among them, the $A_{1g} + 4E_g$ modes are only Raman active, the $3A_{2u} + 5E_u$ are only infrared active and the remaining $2A_{1u} + 3A_{2g}$ are inactive for both Raman and IR spectroscopies [29–31]. The Raman active modes are located at 86, 172, 261, 432 and 584 cm^{-1} at 5 K [29]. However, the spin state of Co^{3+} cations changes from low spin ($t^6_{2g}\, e^0_g$, $S = 0$) to intermediate spin ($t^5_{2g}\, e^1_g$, $S = 1$) state increasing the temperature leading to a structure with mixed low and intermediate states. As the e_g orbitals have a strong Jahn–Teller nature, the local crystal structure changes from rhombohedral $R\bar{3}c$ to monoclinic $I2/a$ (C^6_{2h},) by the Jahn–Teller cooperative effect leading to pronounced modifications of the Raman spectrum [29,31]. In particular, the intensity of the E_g vibration mode at 432 cm^{-1} strongly decreases. This mode is observed around 420 cm^{-1} at room temperature. Additionally, a broad band containing two components is located around 540 cm^{-1}. The observation of a band near 650 cm^{-1} reveals the structural distortion due to the Jahn–Teller effect. Indeed, this

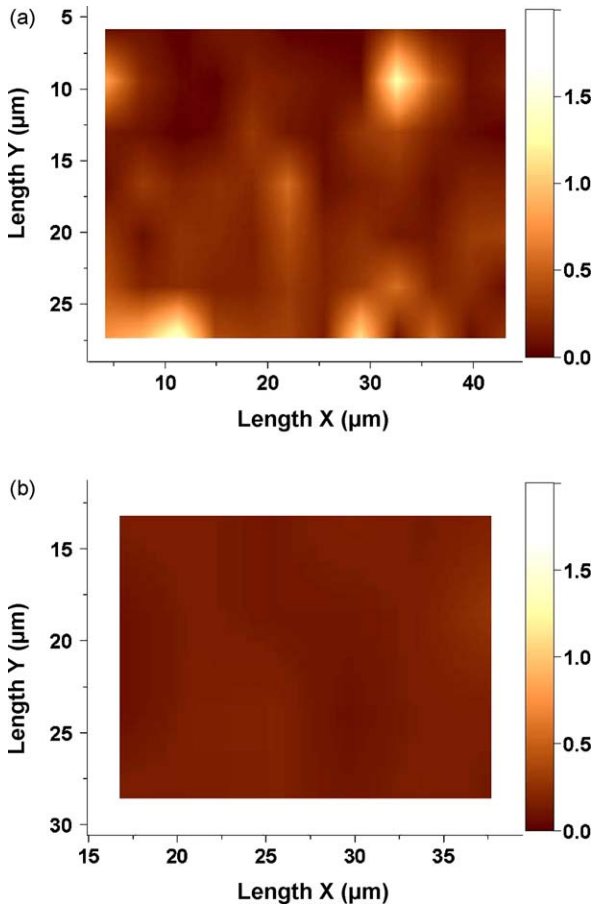

Fig. 6. Raman images plotting the intensity of the band at 690 cm^{-1} of Co_3O_4 for (a) the $La_{0.7}Sr_{0.3}Co_{0.8}Fe_{0.2}O_3$ sample of the first series prepared without titration of nitrates and (b) the $La_{0.7}Sr_{0.3}Co_{0.8}Fe_{0.2}O_3$ sample of the second series prepared with careful titration of nitrates.

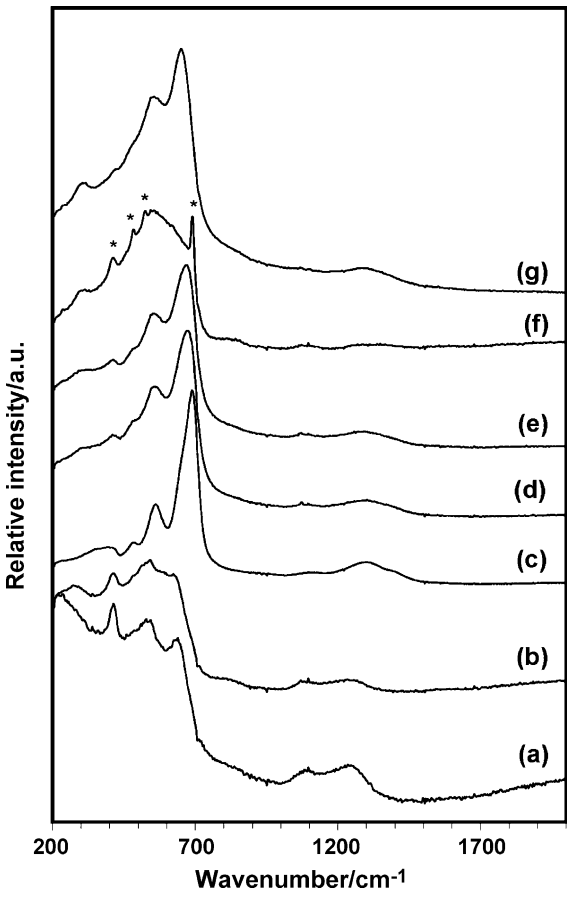

Fig. 7. Raman spectra of the (a) $LaCoO_3$, (b) $La_{0.7}Sr_{0.3}CoO_3$, (c) $LaCo_{0.8}Fe_{0.2}O_3$, (d) $La_{0.7}Sr_{0.3}Co_{0.8}Fe_{0.2}O_3$ (−5% Co), (e) $La_{0.7}Sr_{0.3}Co_{0.8}Fe_{0.2}O_3$, (f) $La_{0.7}Sr_{0.3}Co_{0.8}Fe_{0.2}O_3$ (+5% Co) and (g) $La_{0.7}Sr_{0.3}Co_{0.5}Fe_{0.5}O_3$ samples. *Bands assigned to Co_3O_4 particles.

band assigned to the A_{2g} breathing mode is inactive at 5 K in the $R\bar{3}c$ structure but strongly increase in intensity when the local distortion appears [29].

The mean Raman spectrum of the $LaCoO_3$ sample reported in Fig. 7a shows bands at 417, 540 and 646 cm^{-1} typical of distorted local structure due to the Jahn–Teller effect. The broad bands around 1100 and 1260 cm^{-1} were assigned to overtones. The mean spectrum of the $La_{0.7}Sr_{0.3}CoO_3$ sample (Fig. 7b) was similar but contained broader bands as expected from the smaller crystallite size and the higher surface area. In these two samples, the relative intensity of the band at 646 cm^{-1} varied from one analyzed point to the other indicating local variations of the structural distortion.

The mean spectrum of the $LaCo_{0.8}Fe_{0.2}O_3$ sample (Fig. 7c) was very different from that of the $LaCoO_3$ sample. Indeed, all the bands were shifted to higher wavenumbers and the main band was then located at 692 cm^{-1}. These bands cannot be attributed to any allotropic form of Fe_2O_3 [32,33] nor to Fe_3O_4 [34,35]. However, it could correspond to the band located at 646 cm^{-1} for the $LaCoO_3$ sample (Fig. 7a) and assigned to the A_{2g} breathing mode. In this assumption, its higher intensity would arise from a higher local distortion of octahedra due to substitution of cobalt by iron cations. Similar spectra were observed for the $La_{0.7}Sr_{0.3}Co_{0.8}Fe_{0.2}O_3$ (−5% Co), $La_{0.7}Sr_{0.3}Co_{0.8}Fe_{0.2}O_3$ and $La_{0.7}Sr_{0.3}Co_{0.5}Fe_{0.5}O_3$ samples (Fig. 7d, e and g respectively). The slight red-shift and broadening of bands could be due to the smaller crystallite size. For all these samples, all the recorded spectra during the mappings were close from one point to the other revealing similar local distortions.

Finally, the Raman spectra achieved on the aged samples were close to those on the fresh samples suggesting good thermal stability of the perovskites. In particular, no formation of Co_3O_4 particles was evidenced in the Raman mappings of the pure

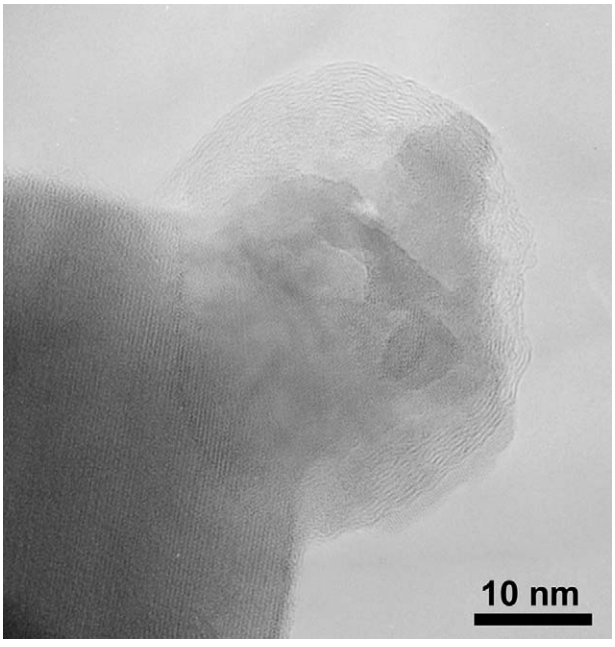

Fig. 8. TEM image of the $La_{0.7}Sr_{0.3}Co_{0.8}Fe_{0.2}O_3$ (+5% Co) sample.

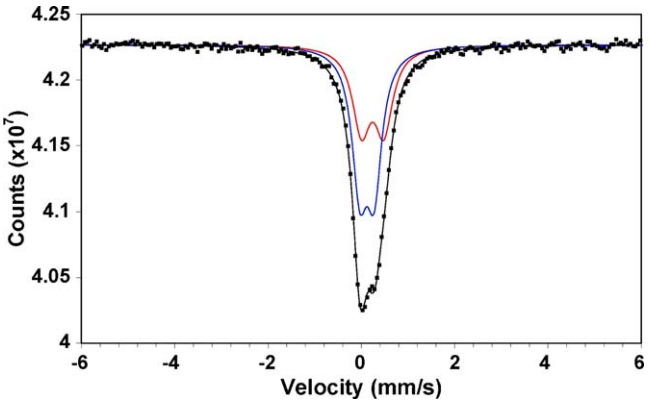

Fig. 9. Mössbauer spectrum of the $La_{0.7}Sr_{0.3}Co_{0.5}Fe_{0.5}O_3$ sample.

perovskites. For the $La_{0.7}Sr_{0.3}Co_{0.8}Fe_{0.2}O_3$ (+5% Co) sample, a similar good dispersion of Co_3O_4 was observed.

The Mössbauer spectrum of the $La_{0.7}Sr_{0.3}Co_{0.5}Fe_{0.5}O_3$ sample plotted in Fig. 9 evidenced two doublets at room temperature corresponding to the signal of Fe^{3+} and Fe^{4+} cations. A slight increase in the proportion of Fe^{4+} cations was observed after catalytic test. No Fe^{5+} cation was evidenced from the Mössbauer spectrum contrary to $La_{0.7}Sr_{0.3}FeO_3$ for which Fe^{4+} cations are disproportionated into Fe^{3+} and Fe^{5+} cations at room temperature [36]. The calculated δ isomeric shifts (referred to α-Fe) were 0.32 and 0.22 mm s^{-1} for the Fe^{3+} and Fe^{4+} cations, respectively and their relative amounts deduced from the peaks areas were 51% and 49%. This result is close to that reported for $La_{0.5}Sr_{0.5}Co_{0.5}Fe_{0.5}O_3$ perovskite [37] and is in agreement with the increase of the *a*, *c* and unit cell volume parameters by substitution of cobalt by iron. It implies that the amount of Co^{4+} cations in this sample was then lower than 10%. Finally, the calculated *D* quadrupolar splitting was 0.48 mm s^{-1} for the Fe^{3+} cations and 0.28 mm s^{-1} for the Fe^{4+} cations confirming the local distortion of octahedra in the perovskite.

The surface composition of $La_{(1-x)}Sr_xCo_{(1-y)}Fe_yO_3$ perovskites was investigated by XPS after treatment under O_2 flow at 600 °C and direct transfer into the analysis chamber. Binding energy values of the Co $2p_{3/2}$ and O 1s peaks and surface atomic ratios are summarized in Table 2. By substitution of lanthanum by strontium cations, a strong increase in oxygen and cobalt amounts were observed. At the same time, the Co $2p_{3/2}$ peak was enlarged and

Table 2
XPS data deduced from spectra of perovskites.

	Atomic ratio			BE (eV)	
	O/La	Co/La	Sr/La	Co $2p_{3/2}$	O 1s
$LaCoO_3$	2.38	0.39	–	780.1	529.0 (46.6%) 530.2 (21.5%) 531.7 (15.4%) 533.0 (16.5%)
$La_{0.7}Sr_{0.3}CoO_3$	7.63	1.11	1.25	780.6	529.0 (32.8%) 530.4 (15.1%) 531.7 (23.0%) 533.1 (29.1%)
$La_{0.7}Sr_{0.3}Co_{0.8}Fe_{0.2}O_3$	7.31	0.93	1.19	780.5	529.0 (34.6%) 530.4 (13.2%) 531.7 (19.5%) 533.2 (32.7%)
$La_{0.7}Sr_{0.3}Co_{0.8}Fe_{0.2}O_3$ without treatment	4.02	0.86	0.32	780.2	528.9 (33.7%) 530.0 (18.6%) 531.4 (44.4%) 532.8 (3.2%)

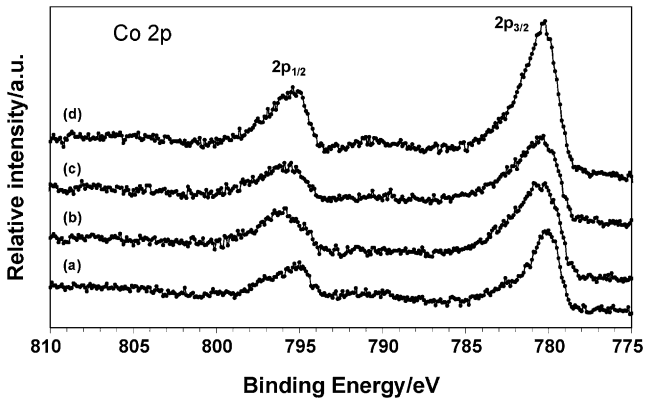

Fig. 10. Co 2p XP spectra of the (a) $LaCoO_3$, (b) $La_{0.7}Sr_{0.3}CoO_3$ and (c) $La_{0.7}Sr_{0.3}Co_{0.8}Fe_{0.2}O_3$ samples after treatment at 600 °C in air and of the (d) $La_{0.7}Sr_{0.3}Co_{0.8}Fe_{0.2}O_3$ sample without treatment.

shifted to higher binding energy values (Fig. 10) suggesting the stabilization of Co^{4+} cations [38,39] in concordance with the decrease in the *a* unit cell parameter deduced from XRD diagrams. No high binding energy satellites at 785–788 eV indicative of the presence of Co^{2+} cations were evidenced [5,40,41].

Fig. 11 compares the O 1s bands of the $LaCoO_3$ and $La_{0.7}Sr_{0.3}CoO_3$ samples. These bands can be decomposed into 4 peaks around 529.0, 530.2, 531.6 and 533.0 eV. The low energy peak was attributed to O^{2-} lattice oxygen species [40] and the high energy one to O^- electrophilic species [40,42,43]. The attribution of the two other bands is not clear in the literature data. They could arise from carbonates [44], hydroxyl groups [40], $(O_2)^-$species [42] or low coordinated oxygen ions located at special site or domains of the surface where the covalence of the M–O bond is higher [45]. A strong enhancement of the relative intensity of the O^- peak was observed for the $La_{0.7}Sr_{0.3}CoO_3$ sample (Fig. 11 and Table 2). It could arise from the raise of the specific surface area and the formation of Co^{4+} cations when La^{3+} was partially replaced by Sr^{2+} cations. By addition of iron cations, an additional enhancement of the amount of O^- species was observed but to a lesser extent (Fig. 11 and Table 2). No other significant difference between the $La_{0.7}Sr_{0.3}CoO_3$ and $La_{0.7}Sr_{0.3}Co_{0.8}Fe_{0.2}O_3$ samples was evidenced by XPS.

Interestingly, the relative intensity of the peak corresponding to O^- species was much lower without treatment (Fig. 11 and Table 2). The difference can be explained by stabilization of O^- species heating the samples at 600 °C. Additionally, the O/La and

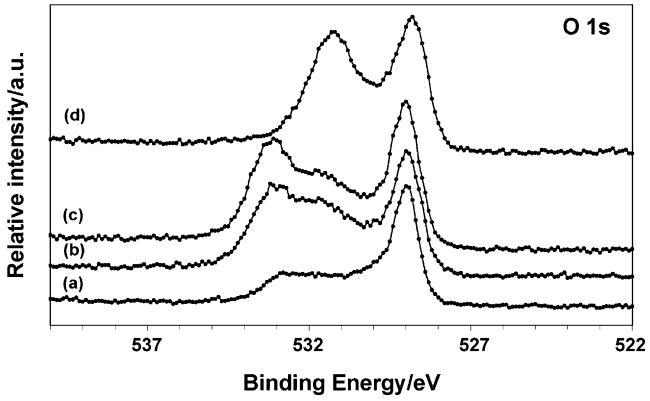

Fig. 11. O 1s XP spectra of the (a) $LaCoO_3$, (b) $La_{0.7}Sr_{0.3}CoO_3$ and (c) $La_{0.7}Sr_{0.3}Co_{0.8}Fe_{0.2}O_3$ samples after treatment at 600 °C in air and of the (d) $La_{0.7}Sr_{0.3}Co_{0.8}Fe_{0.2}O_3$ sample without treatment.

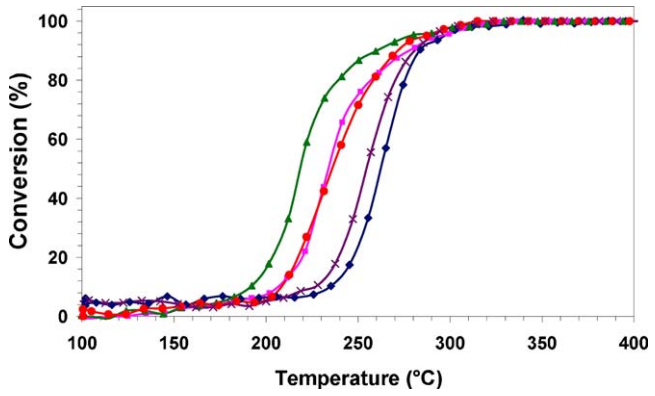

Fig. 12. Toluene conversion versus reactor temperature over the (◆) $LaCoO_3$, (■) $La_{0.7}Sr_{0.3}CoO_3$, (▲) $La_{0.7}Sr_{0.3}Co_{0.8}Fe_{0.2}O_3$, (●) $La_{0.7}Sr_{0.3}Co_{0.5}Fe_{0.5}O_3$ and (×) $LaCo_{0.8}Fe_{0.2}O_3$ samples.

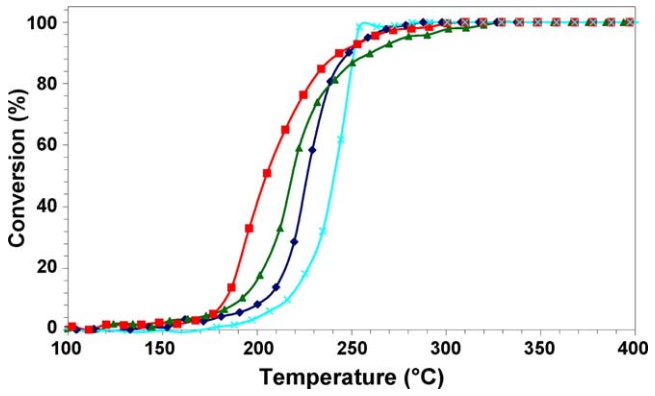

Fig. 13. Toluene conversion versus reactor temperature over the (×) Co_3O_4, (◆) $La_{0.7}Sr_{0.3}Co_{0.8}Fe_{0.2}O_3$ (−5% Co), (▲) $La_{0.7}Sr_{0.3}Co_{0.8}Fe_{0.2}O_3$ and (■) $La_{0.7}Sr_{0.3}Co_{0.8}Fe_{0.2}O_3$ (+5% Co) samples.

Sr/La ratios were much lower without treatment and close to the nominal values confirming the surface modification during the high temperature treatment.

3.2. Catalytic oxidation of toluene

Fig. 12 compares the evolutions of toluene conversions with the reaction temperature for the $LaCoO_3$, $La_{0.7}Sr_{0.3}CoO_3$, $La_{0.7}Sr_{0.3}Co_{0.8}Fe_{0.2}O_3$, $La_{0.7}Sr_{0.3}Co_{0.5}Fe_{0.5}O_3$ and $LaCo_{0.8}Fe_{0.2}O_3$ aged samples. The corresponding T_{20} values and specific activity rates at 220 °C are reported in Table 3. All these samples were active for total oxidation of toluene and complete conversion was reached below 300 °C. The catalytic performances of strontium free perovskites, $LaCoO_3$ and $LaCo_{0.8}Fe_{0.2}O_3$, slightly decreased after the ageing treatment and could be linked to the slight decrease in the SSA values (Table 3). On the contrary, samples substituted with strontium exhibited stable catalytic activities in spite of similar trend for the SSA values. Moreover, performances of $La_{0.7}Sr_{0.3}Co_{0.8}Fe_{0.2}O_3$ were found to be strongly promoted by the thermal treatment on stream at 600 °C. This activation could be linked to the stabilization of O^- species evidenced by XPS after treatment at 600 °C in air and direct transfer into the analysis chamber. The substitution of 30% La^{3+} by Sr^{2+} cations led to a significant improvement of catalytic properties as evidenced by the decrease of 20 °C in the T_{20} values. The doping by iron cations allowed an additional enhancement for an optimized value of 20%. Hence, the best performance was obtained for the $La_{0.7}Sr_{0.3}Co_{0.8}Fe_{0.2}O_3$ sample. Interestingly, the highest specific surface area was also for this sample showing its strong influence on the T_{20} value. However, its specific activity rate was much higher indicating some intrinsic properties were significantly improved (Table 3).

The evolutions of toluene conversions of the $La_{0.7}Sr_{0.3}Co_{0.8}Fe_{0.2}O_3$ (−5% Co), $La_{0.7}Sr_{0.3}Co_{0.8}Fe_{0.2}O_3$, $La_{0.7}Sr_{0.3}Co_{0.8}Fe_{0.2}O_3$ (+5% Co) and reference Co_3O_4 samples are compared in Fig. 13. An additional improvement of catalytic properties was obtained adding 5% of Co in spite of a SSA value that was two times lower. Hence, the specific activity rate was much higher (Table 3). This improvement arises from the presence of small crystallites of Co_3O_4 that was evidenced both by Raman spectroscopy and TEM and cannot be linked to the intrinsic activity of the perovskites. Indeed, several studies report the high catalytic activity of Co_3O_4 catalysts for the total oxidation of CO [46] or hydrocarbons [25–27]. The reference Co_3O_4 sample evaluated in this study was also very active for total oxidation of toluene. Let us note that the T_{20} value of fresh $La_{0.7}Sr_{0.3}Co_{0.8}Fe_{0.2}O_3$ (+5% Co) sample is very similar to that of fresh Co_3O_4. This strongly suggests that the catalytic activity of $La_{0.7}Sr_{0.3}Co_{0.8}Fe_{0.2}O_3$ (+5% Co) is mainly due to the small particles of Co_3O_4 highly dispersed on the perovskite surface. Even if Co_3O_4 is considered as a very effective catalyst for deep oxidation, it suffers of its low thermal stability. It is clearly evidenced in this study since its T_{20} value raised from 195 °C at fresh state to 227 °C at aged state (Table 3). This phenomenon can be explained by the drastic decrease in its SSA value (from 43.6 to 6.9 $m^2\ g^{-1}$) because of sintering of Co_3O_4 particles during the thermal treatment at 600 °C. On the contrary, our method of preparation seems to favour good dispersion of small Co_3O_4 particles with good thermal stability. Indeed, no strong variation of the relative intensity of the Co_3O_4 Raman bands was observed from one point to the other of the Raman mappings achieved on the $La_{0.7}Sr_{0.3}Co_{0.8}Fe_{0.2}O_3$ (+5% Co) sample. Additionally, this good dispersion would be kept after the ageing procedure since the Raman mappings achieved after reaction did not reveal Co_3O_4 sintering. Hence, the T_{20} value of the $La_{0.7}Sr_{0.3}Co_{0.8}Fe_{0.2}O_3$ (+5% Co) sample did not change after the thermal treatment,

Table 3
Comparison of the SSA values, T_{20} temperatures and specific activities at 220 °C of fresh and aged catalysts.

Sample	SSA ($m^2\ g^{-1}$)		T_{20} (°C) fresh	T_{20} (°C) aged	Specify activity rate at 220 °C (10^{-3} μmol s^{-1} m^2) aged
	Fresh	Aged			
$LaCoO_3$	7.4	7.0	225	247	0.84
$LaCo_{0.8}Fe_{0.2}O_3$	9.6	8.9	230	239	1.16
$La_{0.7}Sr_{0.3}CoO_3$	17.1	15.4	216	219	1.38
$La_{0.7}Sr_{0.3}Co_{0.5}Fe_{0.5}O_3$	14.8	14.7	220	217	1.40
$La_{0.7}Sr_{0.3}Co_{0.8}Fe_{0.2}O_3$ (−5% Co)	18.3	17.0	243	214	1.50
$La_{0.7}Sr_{0.3}Co_{0.8}Fe_{0.2}O_3$	22.2	20.0	243	203	2.26
$La_{0.7}Sr_{0.3}Co_{0.8}Fe_{0.2}O_3$ (+5% Co)	10.0	10.1	190	189	5.98
Co_3O_4	43.6[a]	6.9	195	227	1.68

[a] Value measured for the fresh commercial powder.

clearly demonstrating the thermal stability of small Co_3O_4 particles dispersed on lanthanum cobaltite perovskites. At 220 °C and after the ageing step, the intrinsic activity of this catalyst was more than 2.5 and 6 times larger than those recorded on $La_{0.7}Sr_{0.3}Co_{0.8}Fe_{0.2}O_3$ and $LaCoO_3$, respectively.

3.3. Discussion

A series of well-defined $La_{(1-x)}Sr_xCo_{(1-y)}Fe_yO_3$ compounds has been prepared by a citrate–EDTA complexing method. The structural homogeneity and purity of the prepared samples has been carefully checked by Raman mappings. All these perovskites were active for total oxidation of toluene. The ageing procedure used in this study indicated good thermal stability and characterization achieved on the aged samples did not reveal significant modifications.

Comparison with literature is difficult due to different operating conditions (space velocity, toluene/oxygen ratios, etc.). For instance, Deng et al. have investigated the effects of toluene/oxygen molar ratio on the catalytic activity of $La_{0.6}Sr_{0.4}CoO_3$ and have evidenced that the enrichment of O_2 in the reactant feed has a strong positive effect on toluene deep oxidation [47]. Regarding T_{50} values obtained on $LaCoO_3$, i.e. 262 °C, our results are in good agreements with those reported by Irusta et al. [7], i.e. 255 °C, and Alifanti et al. [48] who found 240 °C. Performances recorded on $La_{0.7}Sr_{0.3}Co_{0.8}Fe_{0.2}O_3$ (+5% Co) are significantly better with a T_{50} value equal to 206 °C. Recently, Deng et al. have prepared, by a combined method coupling complexation and hydrothermal processes, various compositions of lanthanum cobaltites and manganites with relatively high specific surface areas [47]. Catalytic performances of these oxides were carried out in operating conditions close to our study (toluene/O_2 molar ratio = 400 and space velocity = 20,000 h^{-1}). They found that the composition $La_{0.6}Sr_{0.4}CoO_3$ was the most suitable for toluene deep oxidation with a T_{20} value of 205 °C and a specific rate of 6.6×10^{-9} mol s^{-1} m^{-2} at 220 °C. These two values are close to those reported in this study for the $La_{0.7}Sr_{0.3}Co_{0.8}Fe_{0.2}O_3$ (+5% Co) sample (Table 3) and confirm that this kind of catalyst is very effective for toluene combustion. Deng et al. [47] did not try to detect the presence of Co_3O_4 by Raman spectroscopy or TEM but have observed by XPS a Co enrichment of the surface of lanthanum cobaltites, which was more pronounced for the most effective composition $La_{0.6}Sr_{0.4}CoO_3$.

It has been previously reported that partial substitution of La^{3+} by Sr^{2+} induces the formation of oxygen vacancies leading to enhancement of the amount of adsorbed oxygen species called α oxygen [10,41] and the formation of a large proportion of Co^{4+} cations [10,49] leading to increase in the electrical conductivity [50]. In this study, X photoelectron spectra indicated that the partial substitution of La^{3+} by Sr^{2+} favours the formation of high amount of O^- electrophilic species especially after treatment at 600 °C in air. These oxidizing species are able to achieve the activation of hydrocarbons [51] which is the limiting step and corresponds to the breaking of the weakest C–H bond in the hydrocarbons [6]. The catalytic activation of the strontium substituted samples observed after the ageing treatment at 600 °C can be explained by stabilization of O^- species that are proposed to be the active sites. These oxygen species would be also responsible of the lowest temperature peak observed by TPD. Indeed, it has been proposed that Co^{3+}–O^- sites could interact with the oxygen adsorbed on low coordination Co^{3+}–O_2^- sites leading to the α_1-desorption process [14].

Partial substitution of cobalt by iron does not affect the amount of adsorbed oxygen species but favours their desorption that occurs at lower temperature as observed from the temperature-programmed desorption (TPD) measurements [10] and could enhance the activity of electrophilic oxygen species. In this study, XRD results suggest that partial substitution of cobalt by iron leads to stabilization of Co^{3+}/Fe^{3+} cations in high spin state or formation of Fe^{4+} cations. The presence of high proportion of Fe^{4+} cations has been evidenced by Mössbauer spectroscopy. In fact, the partial substitution of cobalt by iron induces local structural distortions as evidenced by Raman spectroscopy that could modify the reactivity of the O^- species and explain the improvement of the intrinsic activity of the $La_{0.7}Sr_{0.3}Co_{0.8}Fe_{0.2}O_3$ sample.

4. Conclusions

In this study, well-defined $La_{(1-x)}Sr_xCo_{(1-y)}Fe_yO_3$ perovskites have been prepared by a combined citrate–EDTA complexing method after titration of nitrate precursors. The absence of impurities especially Co_3O_4 that is difficulty detected by XRD has been carefully checked achieving micro-Raman mappings.

All the pure perovskites were very active for total oxidation of toluene above 200 °C and intrinsic activity rates were compared at 220 °C. Partial substitution of La^{3+} by Sr^{2+} cations up to 30% led to a strong enhancement of catalytic properties that arises from both textural and structural modifications. Indeed, it has been shown from BET measurements and SEM characterization such a doping increases significantly the SSA value and changes the shape of primary particles. X photoelectron spectra of samples treated at 600 °C in air and directly transferred into the analysis chamber clearly evidenced the presence of higher amount of O^- electrophilic species that are able to activate hydrocarbons. Stabilization of such species can explain the improvement of intrinsic activity rates when the perovskites are doped by Sr^{2+} cations.

Partial substitution of cobalt by iron up to 20% allowed an additional improvement of the intrinsic activity rate. Textural modifications induced by this doping were rather limited. The amount of O^- measured by XPS was only slightly higher than without iron. However, a strong modification of Raman spectra attributed dynamic structural distortion of oxygen octahedra by Jahn–Teller effect. Additionally, Mössbauer spectra evidenced clearly the presence of both Fe^{3+} and Fe^{4+} cations in the iron containing compounds. These structural modifications could improve the reactivity of O^- species explaining the additional improvement of the intrinsic activity rate.

The T_{20} values of the perovskites without strontium were slightly lower after an ageing treatment at 600 °C for 6 h probably because of the slight decrease in specific surface areas. On the contrary, the strontium containing perovskites exhibited stable or improved T_{20} values. The improvement of catalytic properties observed for the $La_{0.7}Sr_{0.3}Co_{0.8}Fe_{0.2}O_3$ sample could be linked to stabilization of O^- species observed by XPS after similar treatment.

Finally, an additional improvement of catalytic properties was reached adding an excess of cobalt nitrate in the preparation solution. TEM images and Raman mappings revealed the presence of small Co_3O_4 particles that are very active for total oxidation of toluene. Their good dispersion over the perovskite avoided their sintering and allowed to get very efficient and stable catalysts.

Acknowledgements

This work has been achieved within the framework 'Action Concertée Incitative (ACI) Energie, Conception Durable', Grant No. ECD 048, 2004 funded by the French 'Ministère Délégué à la Recherche'. Dr. J.-M. Millet is acknowledged for providing Mössbauer data and M. Daniel for SEM and TEM images. The authors thank also Dr. F. Gaillard for fruitful discussion during ACI meetings.

References

[1] M.F.M. Zwinkels, S.G. Jaras, P.G. Menon, Cat. Rev.: Sci. Eng. 35 (1993) 319.
[2] H. Arai, T. Yamada, K. Eguchi, T. Seiyama, Appl. Catal. 26 (1986) 265.
[3] N.H. Batis, P. Delichere, H. Batis, Appl. Catal. A 282 (2005) 173.
[4] R.J.H. Voorhoeve, in: J.J. Burton, R.L. Garten (Eds.), Advanced Materials in Catalysis, Academic Press, New York, 1977, p. 129.
[5] M. O'Connell, A.K. Norman, C.F. Hüttermann, M.A. Morris, Catal. Today 47 (1999) 123–132.
[6] V. Blasin-Aube, J. Belkouch, L. Monceaux, Appl. Catal. B: Environ. 43 (2003) 175–186.
[7] S. Irusta, M.P. Pina, M. Menedez, J. Santamaria, J. Catal. 179 (1998) 400–412.
[8] J.-J. Liang, H.-S. Weng, Ind. Eng. Chem. Res. 32 (1993) 2563–2572.
[9] C.-C. Chang, H.-S. Weng, Ind. Eng. Chem. Res. 32 (1993) 2930–2933.
[10] H.M. Zhang, Y. Shimizu, Y. Teraoka, N. Miura, N. Yamazoe, J. Catal. 121 (1990) 432–440.
[11] M. Alifanti, J. Kirchnerova, B. Delmon, D. Klvana, Appl. Catal. A: Gen. 262 (2004) 167–176.
[12] G. Busca, M. Daturi, E. Finocchio, V. Lorenzelli, G. Ramis, R.J. Willey, Catal. Today 33 (1997) 239–249.
[14] S. Royer, F. Berube, S. Kaliaguine, Appl. Catal. A: Gen. 282 (2005) 273–284.
[15] M. Alifanti, J. Kirchnerova, B. Delmon, Appl. Catal. A: Gen. 245 (2003) 232–243.
[16] K.R. Barnard, K. Foger, T.W. Turney, R.D. Williams, J. Catal. 125 (1990) 265–275.
[17] Z. Shao, W. Yang, Y. Cong, H. Dong, J. Tong, G. Xiong, J. Membr. Sci. 172 (1–2) (2000) 177–188.
[18] Rodriguez-Carvajal, FULLPROF, version February 05, Laboratoire Leon Brillouin (CEA-CNRS), Saclay, France, 1998.
[19] R.H.E. van Doorn, A.J. Burggraaf, Solid State Ionics 128 (2000) 65–78.
[20] A.N. Petrov, O.F. Kononchuk, A.V. Andreev, V.A. Cherepanov, P. Kofstad, Solid State Ionics 80 (1995) 189–199.
[21] D. Berger, V. Fruth, I. Jitaru, J. Schoonman, Mater. Lett. 58 (2004) 2418–2422.
[22] R.D. Shannon, Acta Crystallogr. Sect. A: Cryst. Phys. Diffr. Theor. Gen. Crystallogr. 32 (5) (1976) 751–767.
[23] N.E. Trofimenko, H. Ullmann, J. Eur. Ceram. Soc. 20 (2000) 1241–1250.
[24] N. Orlovskaya, D. Steinmetz, S. Yarmolenko, D. Pai, J. Sankar, J. Goodenough, Phys. Rev. B 72 (2005) 014122–14131.
[25] A.M. Garrido Pedrosa, M.J.B. Souza, J.D.G. Fernandes, D.M.A. Melo, A.S. Araujo, React. Kinet. Catal. Lett. 79 (2003) 391–396.
[26] U. Zavyalova, P. Scholz, B. Ondruschka, Appl. Catal. A: Gen. 323 (2007) 226–233.
[27] B. Solsona, T.E. Davies, T. Garcia, I. Vazquez, A. Dejoz, S.H. Taylor, Appl. Catal. B: Environ. 84 (1–2) (2008) 176–184.
[28] V. Khadzhiev, M. Lliev, I. Vergilov, J. Phys. C: Solid State Phys. 21 (7) (1988) L199–L201.
[29] A. Ishiwara, J. Nohara, S. Sugai, Phys. Rev. Lett. 93 (13) (2004) 136401–136411.
[30] M.V. Abrashev, A.P. Litvinchuk, M.N. Iliev, R.L. Meng, V.N. Popov, V.G. Ivanov, R.A. Chakalov, C. Thomsen, Phys. Rev. B 59 (6) (1999) 4146–4152.
[31] N. Orlovskaya, D. Steinmetz, S. Yarmolenko, D. Pai, J. Sankar, J. Goodenough, Phys. Rev. B 72 (2005) 014122–14131.
[32] D. Bersani, P.P. Lottici, A. Montenero, J. Raman Spectrosc. 30 (1999) 355–360.
[33] I.V. Chernyshova, M.F. Hochella Jr., A.S. Madden, Phys. Chem. Chem. Phys. 9 (2007) 1736–1750.
[34] Q. Han, Z. Liu, Y. Xu, H. Zhang, J. Cryst. Growth 307 (2) (2007) 483–489.
[35] S. Tiwari, R. Prakash, R.J. Choudhary, D.M. Phase, J. Phys. D: Appl. Phys. 40 (16) (2007) 4943–4947.
[36] S.E. Dann, D.B. Currie, M.T. Weller, M.F. Thomas, A.D. Al-Rawwas, J. Solid State Chem. 109 (1994) 134–144.
[37] F.J. Berry, J.R. Gancedo, J.F. Marco, X. Ren, Hyperfine Interact. 166 (1–4) (2006) 449–453.
[38] H.T. Zhang, X.H. Chen, Nanotechnology 17 (2006) 1384–1390.
[39] J.C. Lupin, D. Gonbeau, H. Benqlilou-Moudden, Ph. Vinatier, A. Levasseur, Thin Solid Films 384 (2001) 23–32.
[40] S. Kaliaguine, A. Van Neste, V. Szabo, J.E. Gallot, M. Bassir, R. Muzychuk, Appl. Catal. A: Gen. 209 (2001) 345–358.
[41] J. Niu, W. Liu, H. Dai, H. He, X. Zi, P. Li, Chin. Sci. Bull. 51 (14) (2006) 1673–1681.
[42] M.W. Roberts, Chem. Soc. Rev. 18 (1989) 451–475.
[43] M.W. Roberts, R. St C. Smart, J. Chem. Soc., Faraday Trans. 80 (11) (1984) 2957–2968.
[44] N.H. Batis, P. Delichere, H. Batis, Appl. Catal. A: Gen. 282 (2005) 173–180.
[45] V.M. Jimenez, A. Fernandez, J.P. Espinos, A.R. Gonzalez-Elipe, J. Electron Spectrosc. Relat. Phenom. 71 (1995) 61–71.
[46] J. Jansson, J. Catal. 194 (2000) 55–60.
[47] J. Deng, L. Zhang, H. Dai, H. He, C.T. Au, Ind. Eng. Chem. Res. 47 (21) (2008) 8175–8183.
[48] M. Alifanti, M. Florea, V. Cortes-Corberan, U. Endruschat, B. Delmon, V.I. Parvulescu, Catal. Today 112 (1–4) (2006) 169–173.
[49] H.M. Zhang, N. Yamazoe, Y. Teraoka, J. Mater. Sci. Lett. 8 (1989) 996.
[50] G. Garcia-Belmonte, J. Bisquert, F. Fabregat, V. Kozhukharov, J.B. Carda, Solid State Ionics 107 (1998) 203–211.
[51] G.I. Panov, K.A. Dubkov, E.V. Starokon, Catal. Today 117 (1–3) (2006) 148–155.